

Contents lists available at ScienceDirect

Petroleum Science

journal homepage: www.keaipublishing.com/en/journals/petroleum-science



Original Paper

Preparation and performance evaluation of a novel sand—water dual-control functional polymer



Tian-Meng Lei ^{a, b, c}, Ye-Fei Wang ^{a, b, c, *}, Xin-Fang Xue ^{a, b, c, d}, Guo-Rui Xu ^d, Ying-Ying Duan ^{a, b, c}, Tian-Ci Ma ^{a, b, c}, Fu-Min Zhang ^{a, b, c}, Shi-Ze Qiu ^{a, b, c}

- ^a State Key Laboratory of Deep Oil and Gas, China University of Petroleum (East China), Qingdao, 266580, Shandong, PR China
- b Key Laboratory of Unconventional Oil □ Gas Development (China University of Petroleum (East China)), Ministry of Education, Qingdao, 266580, Shandong, PR China
- ^c School of Petroleum Engineering, China University of Petroleum (East China), Qingdao, 266580, Shandong, PR China
- ^d Production Optimization, China Oilfield Services Limited, Tianjin, 300452, PR China

ARTICLE INFO

Article history: Received 29 July 2024 Received in revised form 22 October 2024 Accepted 25 October 2024 Available online 26 October 2024

Edited by Yan-Hua Sun

Keywords: Functional polymer Synergistic effect Sand—water dual-control Mechanism analysis

ABSTRACT

In response to the challenges of sand production and high water cut during the exploitation of oil reservoirs in unconsolidated sandstones, a novel sand-water dual-control functional polymer, PDSM, was synthesized using acrylamide (AM), methacryloxyethyltrimethyl ammonium chloride (DMC), and styrene monomer (SM) as raw materials. The chemical structure and thermal stability of PDSM were verified by ¹H-NMR, FT-IR, and TGA analyses. To evaluate its performance, functional polymers PDM and PSM, containing only DMC or SM, respectively, were used as control groups. The study systematically investigated the static adsorption, sand production, sand leakage time, standard water—oil resistance ratio, and water cut reduction performance of PDSM. The results demonstrated that, due to the synergistic effect of functional monomers DMC and SM, PDSM exhibited superior dual-control over sand and water compared to PDM and PSM. PDSM enhanced wettability properties reduce the contact angle of the water phase on oil-wet rock surfaces to 64.0°, facilitating better adsorption of polymer molecules on the rock surface and achieving a static adsorption capacity of 14.6 mg/g. PDSM effectively bridges/bundles sand grains through SM and DMC, increasing resistance to fluid erosion. At a flow rate of 100 mL/min, sand production was only 0.026 g/L, surpassing the "Q/SH 1020 2377-2020" standard for sand inhibitors, which defines "excellent" performance as having a sand production rate of ≤0.05 g/L. PDSM forms an adsorption layer (polymer concentrated layer) on the rock surface, expanding when in contact with water and shrinking when in contact with oil, thereby significantly reducing the permeability of the water layer without affecting the permeability of the oil layer. The standard water—oil resistance ratio was measured at 5.41, and the water cut of produced fluid was reduced by 18.6%. These findings provide new theoretical insights and technical guidance for developing dual-function sand-water control agents. © 2024 The Authors. Publishing services by Elsevier B.V. on behalf of KeAi Communications Co. Ltd. This is an open access article under the CC BY-NC-ND license (http://creativecommons.org/licenses/by-nc-nd/ 4.0/).

1. Introduction

Sandstone reservoirs are characterized by strong heterogeneity, loose cementation, and high porosity and permeability. These properties make them prone to fluid crossflow along high permeability channels, resulting in oil well flooding or premature water production. This leads to an increase in formation water cut, a decrease in capillary forces, and a reduction in formation strength

* Corresponding author.

E-mail address: wangyf@upc.edu.cn (Y.-F. Wang).

(Alakbari et al., 2020; Luo et al., 2022; Seright and Brattekas, 2021). Additionally, fluid shear can damage the grain structure of the formation, leading to sand production (Ross et al., 2006; Zhu et al., 2021a). As sand production progresses, formation strength decreases further, exacerbating heterogeneity and accelerating the ineffective circulation of injected fluids, a phenomenon known as "fingering". This process leads to a rapid increase in the water cut of oil wells (Zhu et al., 2021b, 2021c; Sun et al., 2020a, 2020b). Sand production and high water cut in the formation can have significant negative impacts, including corrosion and blockage of production equipment, damage to wellbore and stratigraphic configuration,

enhanced formation heterogeneity, higher production costs, and environmental pollution. These issues seriously hinder the normal production of oil wells (Marandi et al., 2018; Mishra and Ojha, 2016b; Li et al., 2017).

To address these challenges, operators typically perform separate sand control and water control operations. However, this approach often requires frequent and costly well interventions and lacks a cohesive solution for controlling both sand and water, which restricts efforts to improve and stabilize oil well production (Ivšinović et al., 2022; Liu et al., 2016; Zhao et al., 2015). According to statistics, 48% of oil wells are prone to sand production after water shutoff treatments, and 50% of sand control wells struggle with high water cut, indicating a clear interaction between sand production and water cut that requires simultaneous treatment. Therefore, it is essential to develop an integrated sand—water dual-control technology that combines both sand control and water control capabilities to fundamentally address the issues of sand production and high water cut in oil wells (Deng et al., 2018; Luo et al., 2022; Qiao and Zhu, 2010; Ross et al., 2006).

For integrated sand—water dual-control technology, researchers have developed the widely used resin and cross-linked gel-based agents from a chemical perspective. These agents stabilize and control sand by consolidating sand grains, inhibiting sand production at its source (Mishra and Ojha, 2016a; Saghandali et al., 2022). Additionally, their cementation properties block highpermeability channels, reducing water production in oil wells. These agents offer several advantages, including simple processes, no need for mechanical equipment left in the wellbore, and the ability to perform compensatory operations, thus addressing both the symptoms and root causes of the problem (Safaei et al., 2023; Saghandali et al., 2022). However, they also present certain drawbacks, such as water and oil plugging (reducing oil layers permeability), environmental pollution, and high costs. Moreover, due to the limited pumping time, injecting high viscosity resin/gel solution into the sand producing layers can lead to unsatisfactory results, particularly in formations with permeability below 50 mD (Marandi et al., 2018; Saghandali et al., 2022). Therefore, the development of a sand-water dual-control agent with improved injectability, environmental friendliness, and cost efficiency has become a key research focus.

Cationic polymers can be adsorbed onto the surface of sand grains through electrostatic interaction, utilizing the intermolecular network structure to aggregate the sand grains. Simultaneously, the polymer backbone can shrink in oil and swell in water, effectively plugging water channels without reducing oil permeability, thus providing good dual-control effects for sand and water (Dai et al., 2014; Saghandali et al., 2022; Tabar et al., 2021). The introduction of additional functional monomers with synergistic effects could further enhance the performance of these cationic polymers. For example, hydrophobic monomers can strengthen the intermolecular network structure of cationic polymers through hydrophobic interactions, creating a denser three-dimensional network in solution, which enhances the aggregation of sand grains and improves sand-water dual-control performance (Wang et al., 2011; Ye et al., 2010; Zhu et al., 2021d) (Fig. 1). Li et al. (2017) studied an organic silane condensation polymer, under specific conditions (3%–5% organic silane, 1% HCl catalyst, temperature below 100 °C), formed a hydrophobic film on the surface of sand grains, However, while this polymer exhibited good sand inhibition properties, it lacked water control capabilities. Liu et al. (2016) developed a copolymer of pentaerythritol phosphate melamine salt (PPMS), which effectively altered the ζ potential of solid particles and aggregated sand grains through electrostatic and hydrogen bonding, thereby reducing sand production rate. However, its water control effectiveness remains unknown (Liu et al.,

2016). Dai et al. (2014) synthesized a cationic polymer capable of adsorbing onto the sand layer via electrostatic interactions, effectively plugging high-permeability water layers and reducing the water cut of produced fluids. However, its sand control performance has yet to be evaluated (Dai et al., 2014). Fan et al. (2019) prepared a copolymer of cationic and aromatic monomers that self-aggregate via electrostatic and π - π stacking while exhibiting strong adhesion to seabed rocks via cation- π interactions. Despite this, its sand inhibition and water control performance have not been fully assessed (Fan et al., 2019). Similarly, Li et al. (2022a) studied a poly(4-vinyl pyridine) (P4VP) sand control agent with self-aggregation behavior, which adsorbed and aggregated sand grains through hydrogen bonding and π - π stacking, demonstrating good sand stabilization. However, it lacks water control performance evaluation (Li et al., 2022a)

Although the above studies provide valuable insights, they still struggle to balance sand control and water control performance. Therefore, this paper used a cationic polymer backbone as a chimeric carrier to incorporate hydrophobic monomers, enhancing the intermolecular network structure through associative interactions. A novel sand—water dual-control functional polymer (PDSM) was prepared by copolymerizing acrylamide (AM), methacryloxyethyltrimethyl ammonium chloride (DMC), and styrene monomer (SM). The results indicate that the PDSM exhibits excellent dual-control properties for sand and water, effectively addressing both sand production and high water cut in oil wells with a single application. This provides significant theoretical and practical guidance for developing loose sandstone reservoirs.

2. Experimental materials and procedures

To validate the concept introduced in the introduction, hydrophobic monomers were incorporated into the cationic polymer backbone to enhance synergistic effects between the polymer molecules and sand grains, improving the dual-control performance of the cationic polymer for sand and water (Fig. 1). The experimental materials and procedures are as follows.

2.1. Materials

The following materials were used in the study: acrylamide (AM, 98%), methacryloxyethyltrimethyl ammonium chloride (DMC, AR), styrene monomer (SM, 98%), hydrogen peroxide (HP, AR), sodium formaldehyde sulfoxylate (SFS, AR), 2,2'-azobis(2-methylpropionamidine) dihydrochloride (V50, AR), sodium hydroxide (NaOH, AR), calcium chloride anhydrous (GaCl₂, AR), magnesium chloride hexahydrate (MgCl₂·6H₂O, AR), sodium sulfate anhydrous (Na₂SO₄, AR), sodium bicarbonate (NaHCO₃, AR), potassium chloride (KCl, AR), and sodium chloride (NaCl, AR). The heavy oil used in the study was obtained from the Shengli Oilfield in China, with a viscosity of 206.3 mPa·s at 65 °C under a shear rate of 7.34 s $^{-1}$.

2.2. Synthesis of functional polymer (PDM/PSM/PDSM)

The synthesis process involved dissolving and dispersing AM (21.9 g), DMC (64.0 g), and SM (4.1 g) in 150 mL of deionized water. The pH of the solution was adjusted to 6–7 using aqueous NaOH. After 30 min of N_2 bubbling and cooling the reaction system to below 10 °C, specific amounts of initiators (HP/SFS, V50) were added. The low reaction temperature was maintained for 6 h, followed by heating to 50 °C for an additional 2 h to form a copolymer gel (PDSM). The gel was then prepared into a solution and dialyzed using a dialysis bag in deionized water for 3 days. Finally, it was vacuum freeze-dried at -50 °C to obtain a white powder.

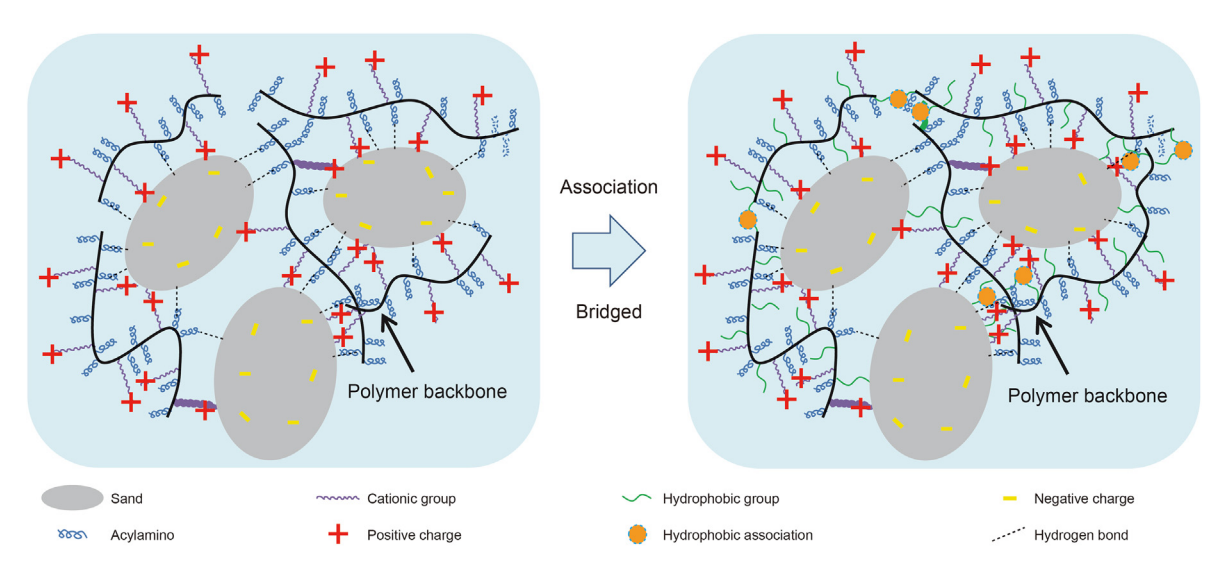


Fig. 1. Mechanism schematic of sand control by cationic polymers with hydrophobic groups.

Throughout the process, the total mass fraction of the reaction monomer was maintained at 60%. The synthetic methods for producing PDM (M_{AM} : $M_{DMC} = 50$:50), PSM (M_{AM} : $M_{SM} = 94$:6), and PDSM (M_{AM} : M_{DMC} : $M_{SM} = 47$:47:6) are shown in Fig. 2.

Considering that polymer abbreviations are typically

represented by P"X"M. Therefore, we named the copolymer of AM and SM as PSM, where "S" means the functional monomer SM; the copolymer of AM and DMC is named PDM, where "D" represents the functional monomer DMC. Finally, the copolymer of AM, DMC, and SM is named PDSM, with "D" and "S" representing the

Fig. 2. Synthesis of PDM (a), PSM (b), and PDSM (c).

functional monomers DMC and SM, respectively.

2.3. Evaluation of polymer properties

2.3.1. Molecular structure characterization

 1 H-NMR spectroscopy was carried out using an AVANCE NEO 500M spectrometer with $D_{2}O$ as the solvent. Fourier transform infrared spectroscopy (FT-IR) was performed using an IFS 125 HR infrared spectrophotometer. Thermogravimetric (TGA) was performed using an STA449F3 thermogravimetric analyzer.

2.3.2. Solution performance

Apparent viscosity: The preparation method of functional polymer solution followed the China Petroleum and Natural Gas Industry Standard SY/T 5862-2020. The apparent viscosity of the functional polymer solution was measured using a BROOKFIELD viscometer (DV2TLVTJO) under the experimental conditions of 65 °C and a shear rate of 7.34 s $^{-1}$. The salt ion composition of the simulated water is shown in Table 1.

Wettability change: Rock slices were soaked in kerosene and aged for 72 h under high-temperature and high-pressure conditions. At this point, the surface of the rock slice achieved in the oilwet state. A high-temperature and high-pressure contact angle measuring instrument (SL200HP) was then used to measure the contact angle of functional polymer solution droplets onto oil-wet rock slices. A contact angle between 0° and 90° indicates a waterwet state, while angles between 90° and 180° indicate an oil-wet state.

Static adsorption: Quartz sand (20.0 g; 0.120–0.180 mm) and functional polymer solution (100 g) were placed in a 150-mL conical flask. The mixture was left to equilibrate for 24 h to equilibrate, with shaking every hour to ensure thorough contact. The upper clear liquid was removed and centrifuged for 20 min at 4000 rpm. The concentration C of the functional polymer in the equilibrated solution was then determined using a UV spectrophotometer (PerkinElmer LAMBDA 365, $\lambda = 202.2$ nm) after calibration (Shi et al., 2020; Zhao et al., 2017; Huang et al., 2018). The adsorption capacity F (mg of polymer adsorbed per gram of sand) was then calculated according to Eq. (1)

$$F = \frac{(C_0 - C)V_p}{m_s} \tag{1}$$

where C_0 is the initial concentration of the functional polymer before adsorption, mg/L; C is the concentration of the functional polymer after adsorption, mg/L; V_p is the volume of functional polymer solution used, L; m_s is the mass of the quartz sand used, g.

The surface microstructure of rock slices after being immersed in the functional polymer solution for 24 h was observed using a scanning electron microscope (SEM).

2.3.3. Sand inhibiting performance

Sand production rate: A mixture of quartz sand $(0.380-0.830 \, \text{mm})$ and kaolin $(0.050-0.071 \, \text{mm})$ in a mass ratio of 21.2:1 was fully mixed and packed into a sand-filled pipe $(\Phi 2.5 \, \text{cm} \times 10 \, \text{cm})$ and compacted. First, the sand-filled pipe was saturated with simulated water in the forward direction. Then, 2

pore volumes (PV) of functional polymer solution were reverse-injected and aged for 24 h (65 °C, 1 mL/min). After aging, 100 mL of simulated water was forward-injected at a rate of 100 mL/min for 1 h. The produced liquid was collected and filtered, and the solids were dried. The sand production rate was calculated according to Eq. (2). This experiment was performed with reference to the Chinese invention patent of "A New Method for Evaluating Polymer Sand Inhibitor Suitable for Large Displacement Production Conditions in Offshore Oilfields" (CN118275289A).

$$Q = \frac{m_2 - m_1}{V_f} \tag{2}$$

where Q is sand production rate, g/L; m_1 is the mass of the filter paper, g; m_2 is the mass of the filter paper and filter residue, g; and V_f is the volume of the filtrate, L.

Critical flow rates for sand production: The same experimental procedures outlined in Section "Sand production rate" were followed until the sand-filled pipe completed the aging process. The screens at the pipe outlet were then removed, and simulated water was forward-injected at an initial rate of 1 mL/min. The flow rate was gradually increased in 0.5 mL/min increments. The point at which sand production began (observed as a white turbid liquid) was recorded as the critical flow rate for sand production.

Sand leakage time: A total of 75.0 g of quartz sand (0.125–0.178 mm; 80–120 mesh) was placed into the separatory funnel (250 mL), followed by the slow addition of 100.0 g of the functional polymer solution. The funnel was sealed and put in an oven for aging at 65 °C for 2 h. The time taken for the sand particles to completely leak out of the funnel was recorded. This experiment was performed with reference to the Chinese invention patent of "A Rapid Method for Evaluating the Performance of Sand Inhibitor" (CN118329696A).

2.3.4. Water control performance

Standard water—oil resistance ratio (N_{FRR}): Two sand-filled pipes with the same permeability were prepared and labeled 'core C1' and 'core C2'. The cores C1 and C2 were saturated with simulated water and crude oil, respectively. The permeabilities $K_{\text{W(C1)}}$ and $K_{\text{O(C2)}}$ were measured during stable injection. Next, 0.5 PV of functional polymer solution was reverse-injected into both cores and aged for 24 h. After aging, simulated water (C1) and crude oil (C2) were injected, and the post-treatment permeabilities, $K_{\text{W(C1)}}$ ' and $K_{\text{O(C2)}}$ ', were recorded under stable injection conditions. The residual resistance factor (F_{RR} , dimensionless) and standard water—oil resistance ratio (N_{FRR} , dimensionless) were calculated (1 mL/min, 65 °C) according to Eqs. (3) and (4):

$$F_{\rm RR} = \frac{K}{K'} \tag{3}$$

$$N_{\rm FRR} = \frac{F_{\rm RRw}}{F_{\rm RRo}} \tag{4}$$

where K is the permeability during the first saturation step, D; K' is the permeability after the functional polymer injection, D; F_{RRw} is the residual resistance coefficient of the water-bearing core C1,

Table 1Salt ion composition of simulated water.

Ion concentration, mg/L							
$K^+ + Na^+$	${\rm Mg}^{2+}$	Ca ²⁺	Cl-	SO ₄ ²⁻	HCO ₃ ²⁻		
4856.5	594.5	134.0	8937.0	1283.0	87.0	15937.0	

dimensionless; and F_{RRo} is the residual resistance coefficient of the oil-bearing core C2, dimensionless.

Water cut reduction in produced fluid: Two sand pipes with permeabilities of 1000 and 2000 mD (±50 mD) were connected in parallel to evaluate the performance of the functional polymer in reducing the water cut of produced fluids. The experiment proceeded as follows: (1) The sand-filled pipes were vacuumed and saturated with simulated water, and their porosity and permeability were measured. (2) The sand pipes were saturated with crude oil and aged 72 h at 65 °C. (3) Simulated water was forward-injected until the water cut of the produced fluid reached 96%. (4) Subsequently, 0.5 PV of the functional polymer solution was reverse-injected into the pipes, and the system was aged for 24 h. (5) Finally, simulated water was forward-injected again until the water cut of the produced liquid reached 96% (1 mL/min, 65 °C). This method follows the standard SY/T 5862—2020 of the Chinese Petroleum and Natural Gas Industry.

3. Results and discussion

3.1. Molecular structure characterization

3.1.1. ¹H-NMR spectra

The ¹H-NMR spectra of PSM, PDM, and PDSM are shown in Fig. 3. The peaks at a ($\delta=1.2$ ppm), b ($\delta=1.6$ ppm), and c ($\delta=2.1$ ppm) correspond to the characteristic H atoms of methyl, methylene, and methine on the polymer backbone, respectively. Peaks d ($\delta=3.2$ ppm), e ($\delta=3.4$ ppm), and f ($\delta=4.0$ ppm) represent the methyl and methylene groups on the quaternary ammonium group, as well as the characteristic peaks of the H atom in the methylene group connected to the ester group. Additionally, peak g ($\delta=7.2-7.6$ ppm) is the characteristic signal of the H atom on the benzene ring. These results confirm the successful grafting of SM and DMC onto the polymer backbone.

3.1.2. FT-IR spectra

The FT-IR spectra of PSM, PDM, and PDSM are shown in Fig. 4. Locations 1 (σ = 706.65 cm $^{-1}$) and 2 (σ = 764.19 cm $^{-1}$) correspond to the =C-H characteristic of the benzene ring. Locations 3 (σ = 951.23 cm $^{-1}$) and 4 (σ = 1081.85 cm $^{-1}$) are attributed to the

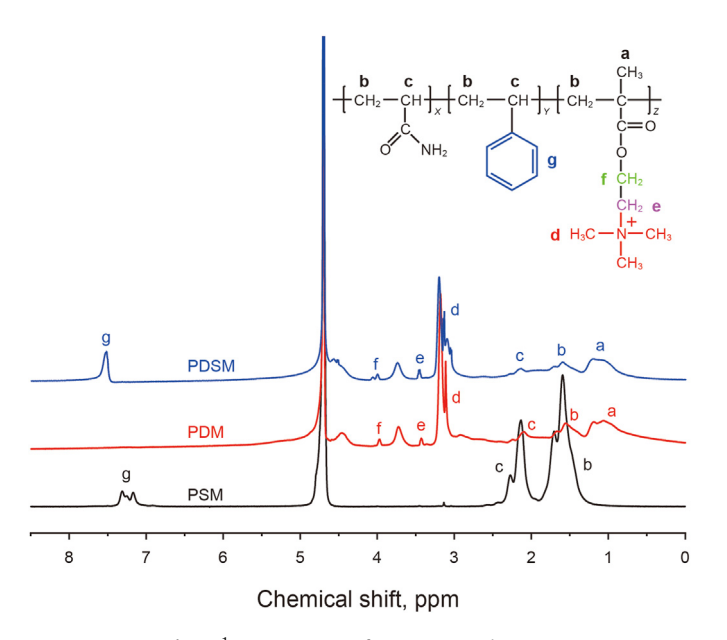


Fig. 3. ¹H-NMR spectra of PSM, PDM, and PDSM.

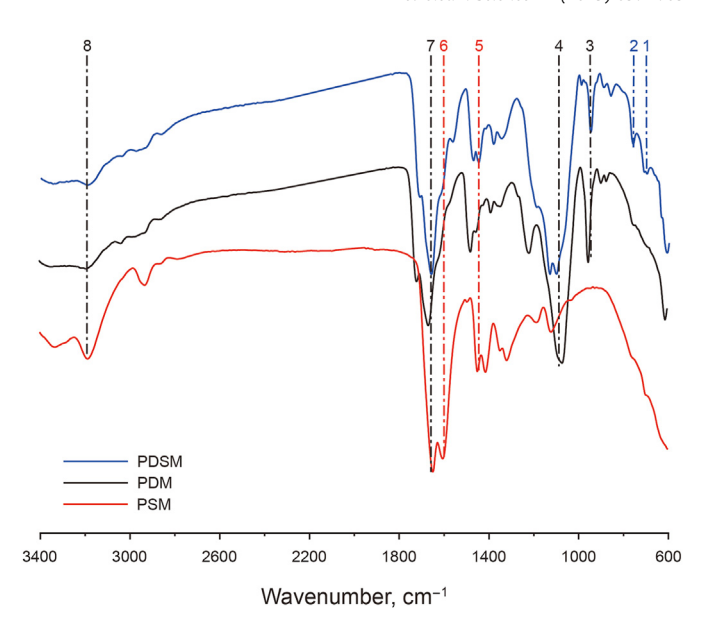


Fig. 4. FT-IR spectra of PSM, PDM, and PDSM.

quaternary ammonium group $(-N^+(CH_3)_3)$ and ester group (-COOC-), respectively. Locations 5 ($\sigma=1451.60~cm^{-1}$) and 6 ($\sigma=1603.25~cm^{-1}$) represent the -C=C- characteristic peaks of the benzene ring. Locations 7 ($\sigma=1662.76~cm^{-1}$) and 8 ($\sigma=3186.32~cm^{-1}$) correspond to the characteristic peaks of -C=O and $-NH_2$ of the amide group, respectively. These results indicate that PSM, PDM, and PDSM were all target products.

3.1.3. Thermogravimetric analysis (TGA)

The thermogravimetric analysis (TGA) curves of PDM, PSM, and PDSM are shown in Fig. 5. Increasing temperature from 30 to 110 °C, the functional polymers show partial weight loss, attributed to the evaporation of free water adsorbed by the hydrophilic groups in the molecular chain of the functional polymers (Chen et al., 2023). From 110 to 220 °C, the weight of the functional polymer remains relatively stable. Further increasing temperature to 350 °C, the amide groups, quaternary ammonium groups, and benzene rings in

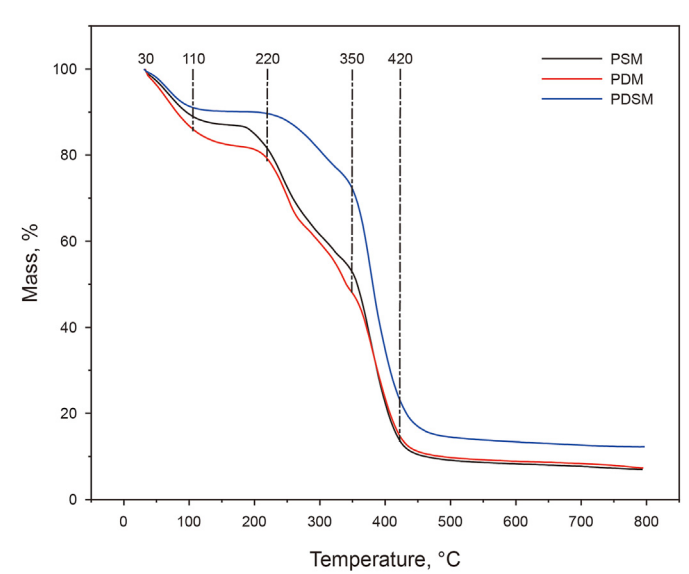


Fig. 5. TGA curves of PSM, PDM, and PDSM.

the molecular chain of the functional polymer degrade significantly, with weight losses of PSM, PDM, and PDSM were 30.8%, 23.0%, and 13.6%, respectively. At this stage, PDSM retains 76.5% of its mass, which is higher than PSM (56.1%) and PDM (58.9%). From 350 to 420 °C, the polymer backbone begins to degrade, and the weight loss of the functional polymer reaches 50%. By 800 °C, PDSM retains 12.3% of its mass, higher than PSM (7.0%) and PDM (7.3%). The results indicate that PDSM exhibits superior thermal stability compared to PSM and PDM.

3.2. Solution performance

3.2.1. Apparent viscosity

To clarify the critical association concentrations (CACs) and injectivity of the functional polymers, the apparent viscosity of polymer solutions at different concentrations was measured and the results are shown in Fig. 6. The CAC helps determine the optimal concentration for practical use, as better results are obtained when the concentration exceeds the CAC value. Injectivity indicates whether the polymer meets field application requirements; for instance, Bohai Oilfield requires the apparent viscosity of a sand—water dual-control agent to be less than 50 mPa·s.

As the concentration increases, the viscosity of the functional polymer solutions gradually increases. When the concentration exceeds 2500 mg/L, the viscosity of PSM and PDSM solutions increases significantly, indicating the formation of macromolecular aggregates and a three-dimensional network structure dominated by intermolecular associations. This suggests that the CACs of PSM and PDSM are 2500 mg/L (Lei et al., 2024; Chen et al., 2023). Compared to PDM and PSM, the solution viscosity of PDSM is higher due to the presence of two functional monomers, which enhance the intermolecular interaction (hydrogen bond, π - π , cation- π , π -cation- π) and form a denser spatial network structure (Li et al., 2015; Wang et al., 2011; Gebbie et al., 2017). At the concentration of 5000 mg/L, the viscosity of PDSM solution is approximately 45.7 mPa·s, indicating that it has good injectivity at high concentrations and meets the requirements for field use as a sand-water dual-control agent.

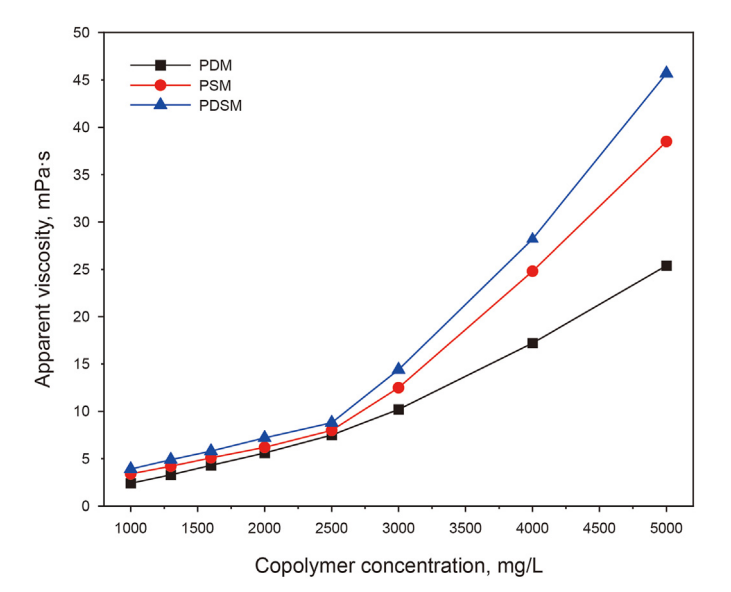


Fig. 6. Solution viscosity of functional polymers at different concentrations.

3.2.2. Wettability alteration

Because the adsorption capacity of the polymer on the waterwet surface is significantly greater than that on the oil-wet surface, this factor can have a substantial impact on the effectiveness of sand—water dual-control. The contact angle is an essential parameter in evaluating the wettability alteration. Thus, it is necessary to measure the contact angle θ of functional polymers on oil-wet rock surfaces (Ahmed et al., 2020; Chiappa et al., 1999; Fan et al., 2019; Safaei et al., 2023).

As shown in Fig. 7, the contact angle between PDSM and oil-wet rock surface is 64.0°, significantly lower than that of PDM and PSM. This indicates that PDSM is more effective at altering the wettability of the rock surface and promoting the transformation of the rock surface from oil-wet to water-wet. Because PDSM contains two functional monomers that not only form strong interactions with rock surfaces but also have a good affinity for heavy oil, the benzene ring in PDSM can interact strongly with gum and asphaltene in heavy oil (Ai-shajalee et al., 2021; Lei et al., 2024; Qin et al., 2020), making it easier for PDSM molecules to spread on the surface of oil-wet rock, reduce the oil-water contact angle and alter the wettability of the rock.

3.2.3. Static adsorption

Since the adsorption capacity of functional polymers on the surface of sand grains is related to their sand inhibition performance (generally, a larger adsorption capacity indicates better sand inhibition, while a smaller capacity suggests poorer performance), the static adsorption performance of PSM, PDM, and PDSM was investigated.

Firstly, the functional polymer solution with known concentration was prepared, and the standard curve fitting equations of PSM, PDM, and PDSM were obtained by measuring their absorbance (5–100 mg/L). The results are shown in Fig. 8(a). To measure the absorbance of a functional polymer solution that has reached adsorption equilibrium, the dilution method is used to ensure that the concentration of the test solution falls within the standard curve range (Shi et al., 2020; Zhao et al., 2017; Huang et al., 2018).

The isothermal adsorption curves of PSM, PDM, and PDSM are shown in Fig. 8(b). As the concentration increases, the adsorption capacity of PDM, PSM, and PDSM on the surface of sand grains increases gradually. When the concentration increases to 4000 mg/ L, the adsorption capacity level off. This behavior occurs because, at low concentrations, the functional polymer is adsorbed on the surface of sand grains, leaving many activated adsorption sites still available and resulting in a lower adsorption capacity. As the concentration increases, more functional polymer molecules adsorb onto the surface of the sand grains, thereby increasing adsorption capacity. Once adsorption sites are fully occupied, further increases in concentration do not result in additional adsorption, leading to saturation (Zhao et al., 2017; Huang et al., 2018). Compared to PDM (8.7 mg/g) and PSM (0.8 mg/g), PDSM exhibited a higher maximum adsorption capacity, reaching 14.6 mg/g. This superior performance is due to the presence of both DMC and SM in PDSM, whose synergistic effects enhance the interaction between the polymer molecules and sand grains, further promoting adsorption (Zhu et al., 2021d; Qin et al., 2020).

To further investigate the adsorption behavior of functional polymer on the surface of sand grains (replaced with rocks), the microstructure of rock slices after treated with functional polymer solutions was observed via scanning electron microscopy (SEM) at 5000 mg/L concentration. The results, shown in Fig. 9, indicate that compared with PDM and PSM, the molecular coil dimension (aggregate) formed by PDSM on the rock surface is large in size, and

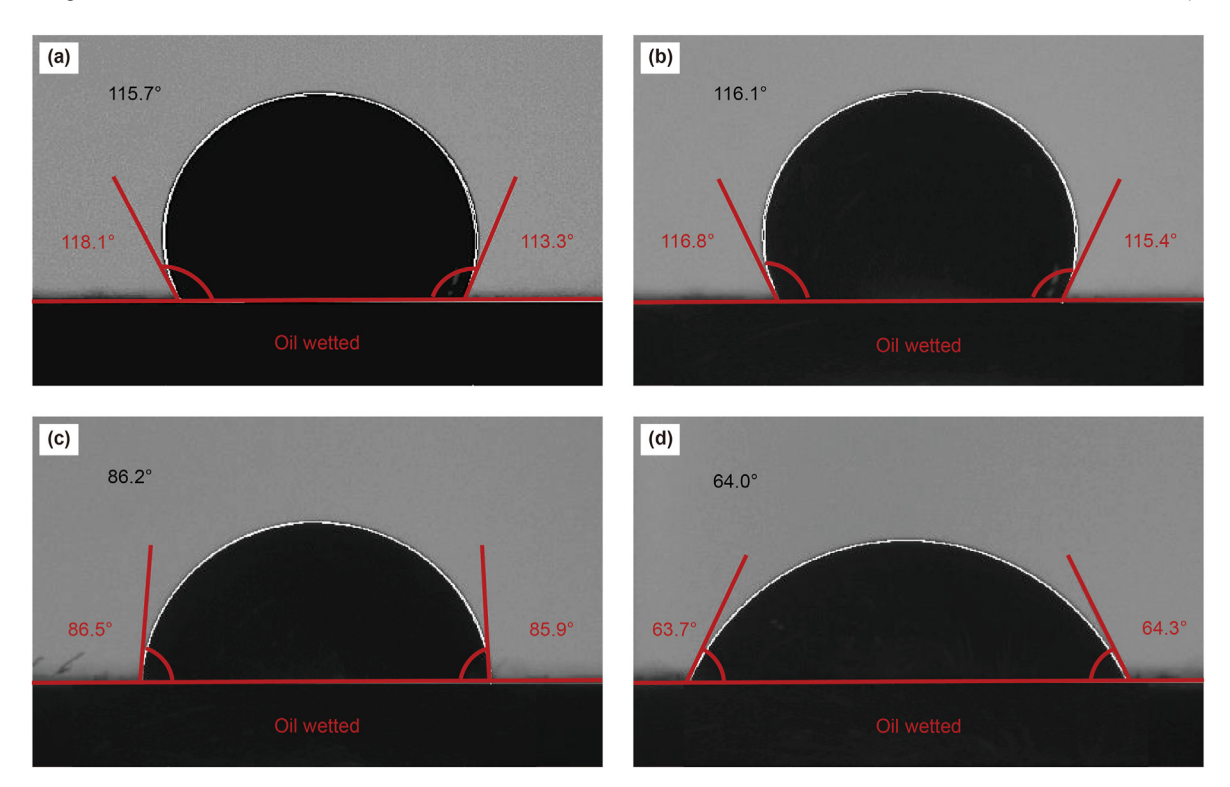


Fig. 7. Contact angle of simulated water (a), PDM (b), PSM (c), and PDSM (d) on oil-wet rock surfaces (5000 mg/L).

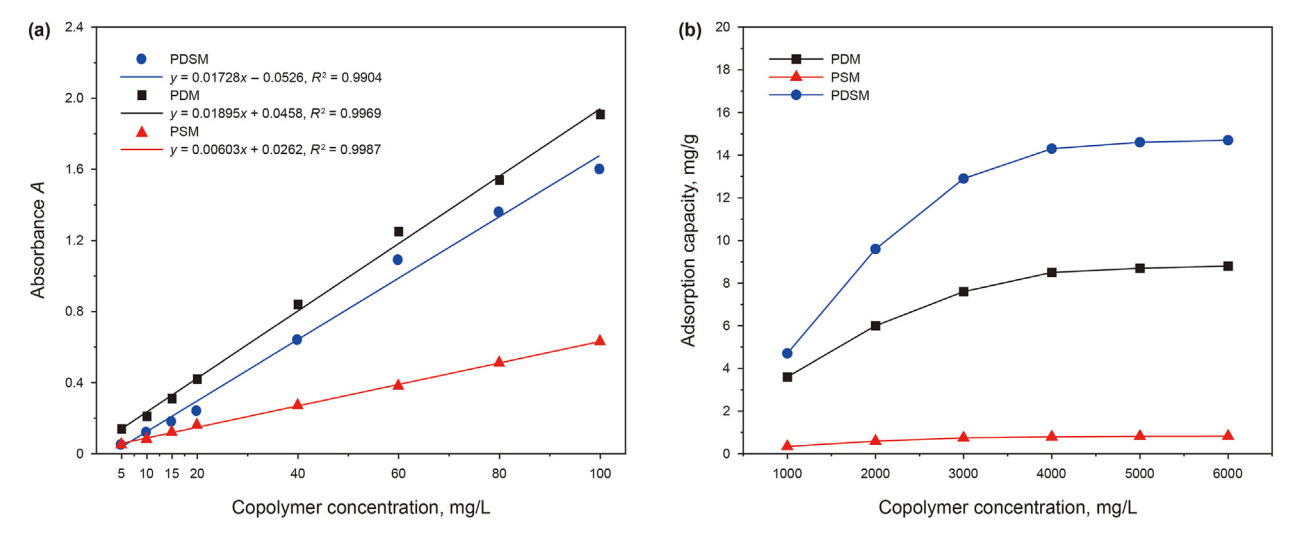


Fig. 8. Standard curves (a) and adsorption capacity (b) of functional polymers at different concentrations.

the resulting adsorption layer is thicker. These findings are consistent with the static adsorption performance trends of functional polymers.

3.3. Sand inhibiting performance

3.3.1. Sand production rate

In the industry, a standard method to evaluate the performance of sand inhibitors is to measure their sand production rate under specific conditions. According to enterprise standard Q/SH 1020 2377-2020 of the China Petrochemical Group Co., Ltd, a sand inhibitor is considered to have "excellent" performance if its sand production rate is $\leq 0.05~\text{g/L}$. The sand production rates of

functional polymers with different concentrations are shown in Fig. 10.

As the concentration increases, the sand production of PDM, PSM, and PDSM gradually decreases. Compared to PSM, both PDM and PDSM exhibit lower sand production rates due to the presence of cationic groups that can generate electrostatic interactions with sand grains (Dai et al., 2014; Howard et al., 1977; Liu et al., 2016). At a concentration of 5000 mg/L, the sand production rate of PDSM is 0.026 g/L, which was 61.7% and 38.1% lower than that of PSM and PDM, respectively, demonstrating excellent sand inhibiting performance. This behavior is attributed to the synergistic effect of DMC and SM, which helps PDSM form a three-dimensional network structure on the rock surface, effectively stabilizing the

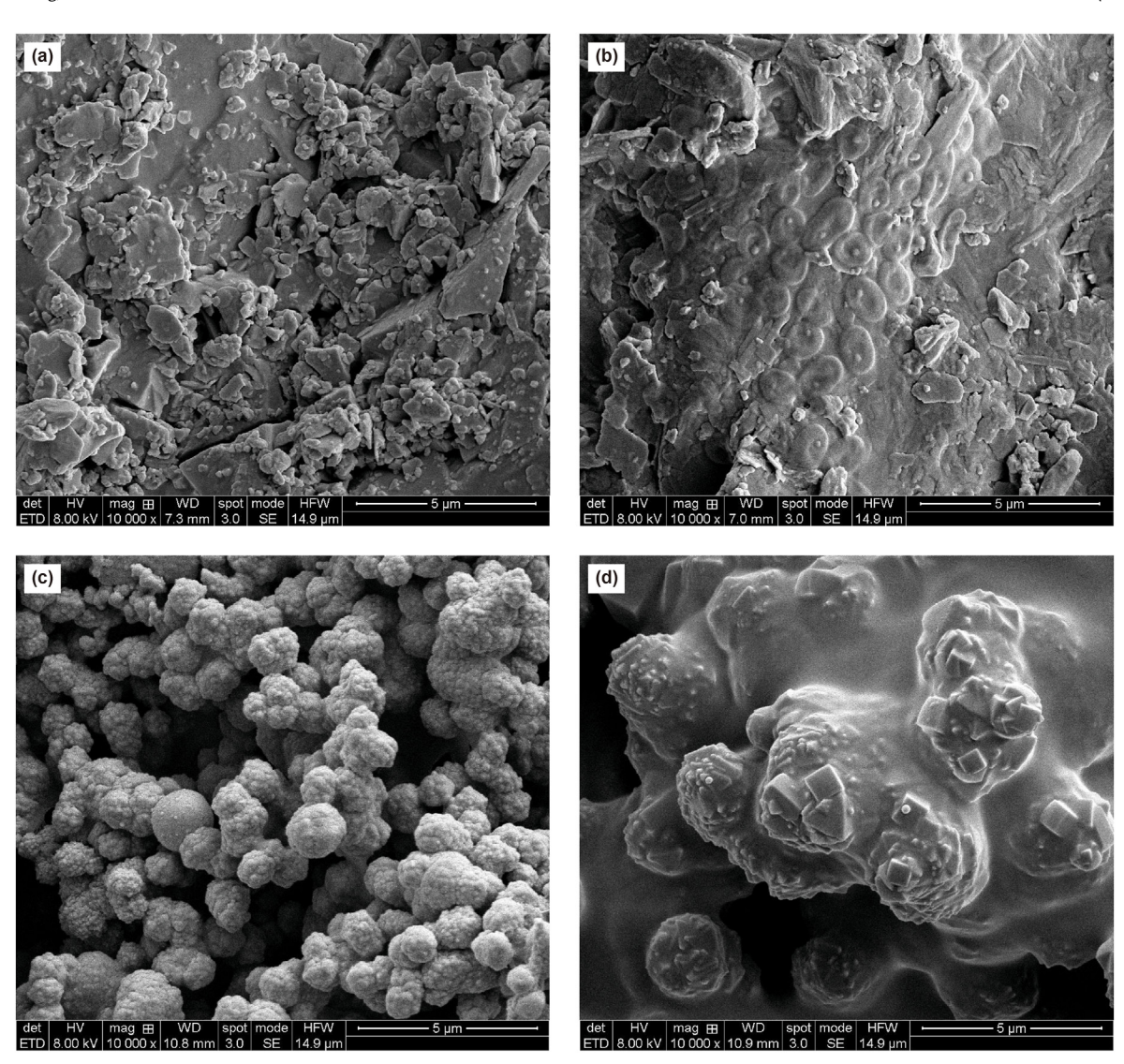


Fig. 9. Microstructures of the rock surface without adsorption of polymer (a) and adsorbed by polymer (b: PSM; c: PDM; d: PDSM).

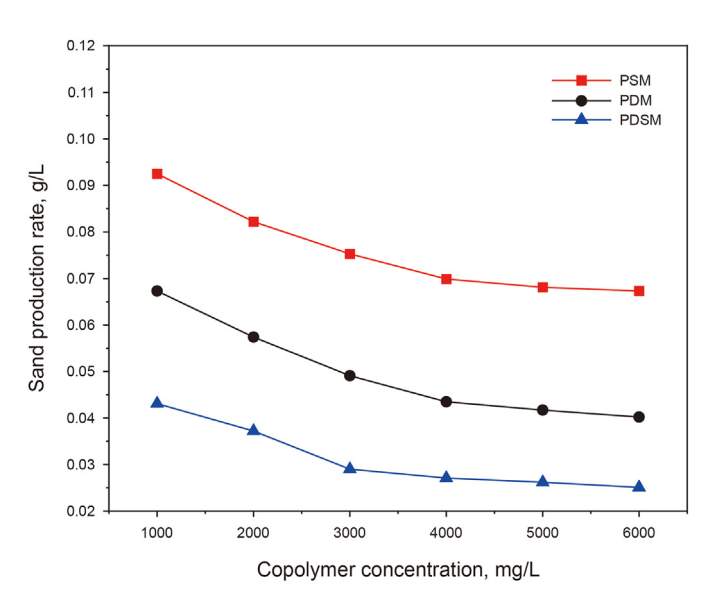


Fig. 10. Sand production rates of functional polymers at different concentrations.

sand grains and making them more resistant to the shear forces caused by fluid flow (Howard et al., 1977; Fan et al., 2019).

3.3.2. Critical flow rate for sand production

During the exploitation of loose sandstone reservoirs, there is a critical flow rate for sand production. No sand is produced when the displacement flow rate is less than the critical sand production flow rate. However, when the flow rate exceeds this threshold, the stable state between the sand grains is disrupted, leading to sand production in the formation. The sand inhibitors can increase the critical sand production flow rate of an oil reservoir by agglomerating and stabilizing the sand grains. The higher the critical flow rate, the better the sand inhibiting performance. Therefore, the critical sand production flow rates of functional polymers with different concentrations are shown in Fig. 11.

As the concentration increases, the critical flow rates for sand production of PDM, PSM, and PDSM initially increase and then stabilize. At low concentrations, incomplete adsorption of polymer molecules leaves active adsorption sites vacant on the surface of sand grains, limiting performance. As the concentration increases, these sites become fully occupied, enhancing sand inhibiting performance and increasing the critical flow rate. Once adsorption

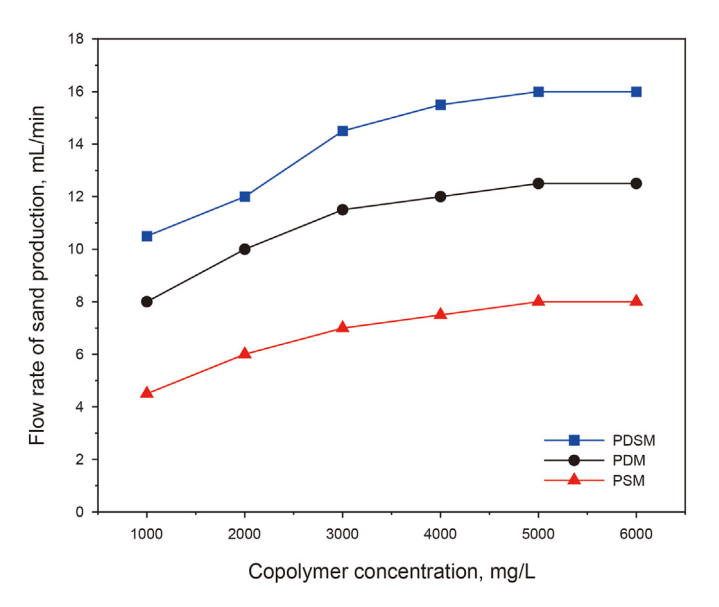


Fig. 11. Critical sand production flow rates of functional polymers at different concentrations.

saturation is reached, further increase in concentration does not significantly affect the critical flow rate (Nejati et al., 2023; Pereira and Delpech, 2012). As the concentration increases from 1000 to 5000 mg/L, the maximum critical sand production flow rate of PDSM is 16.0 mL/min, which is higher than PDM (12.5 mL/min) and PSM (8.0 mL/min). This improvement is due to the synergistic effect of the two functional monomers in PDSM, which enhances the adsorption and bridging effect on sand grains, improving the agglomeration of sand grains and increasing the critical flow rate (Fan et al., 2019; Howard et al., 1977).

3.3.3. Sand leakage time

To rapidly assess the sand inhibiting performance of different functional polymers, we established a sand leakage time evaluation method. This method is simpler and faster than the sand production rate test and it has a good correlation consistency with the sand inhibitor evaluation standard "Q/SH 1020 2377-2020".

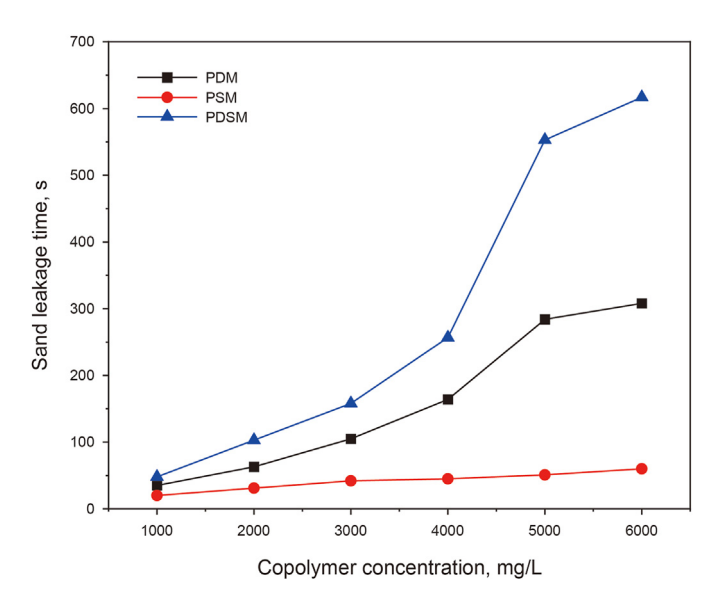


Fig. 12. Sand leakage times of functional polymers at different concentrations.

Generally, the longer the sand leakage time, the better the sand stability performance.

The sand leakage times of functional polymers with different concentrations are shown in Fig. 12. As the concentration increases, the sand leakage time of PDM and PDSM significantly increases. At a concentration of 5000 mg/L, the sand leakage time of PDSM and PDM reach saturation state, showing no further increase with higher concentrations. This behavior is likely due to two factors: (1) The polymer reaches adsorption saturation on the surface of the sand grains at 5000 mg/L. (2) The interactions (association, hydrogen bond, electrostatic) between polymer molecules and sand grains stabilize, preventing further vertical movement of the sand grains. At a concentration of 5000 mg/L, the sand leakage time of PDSM is 553 s, much higher than that of PSM and PDM. The presence of two functional monomers in PDSM creates stronger interactions with sand grains, enhancing the agglomeration of the grains, inhibiting their movement, and prolonging the sand leakage time. Therefore, PDSM has better sand stabilization performance (Li et al., 2022a; Shi et al., 2020).

To further investigate the properties of the adsorption layer formed between the polymers (at 5000 mg/L) and the sand grains, the mixtures formed during the sand leakage experiments were allowed to stand for 3–5 days. The results are shown in Fig. 13. Compared to PSM and PDM, the adsorption layer (polymer concentrated layer) formed by PDSM on the surfaces of sand grains is thicker, and the solution above the sand was also much clearer. This suggests that fewer free polymer molecules remain in the solution, allowing more molecules to adsorb onto the sand grain surface, resulting in better sand inhibiting performance.

3.4. Water control performance

3.4.1. Standard water—oil resistance ratio (N_{FRR})

To access the selective water control performance (water plugging without oil plugging) of the functional polymers, we evaluated the standard water—oil resistance ratio ($N_{\rm FRR}$) established by three functional polymers. $N_{\rm FRR}$ is one of the most effective indicators for selective water control performance, with a higher $N_{\rm FRR}$ value indicating better performance that polymer preferentially blocks water flow over oil flow.

The results of the selective water control experiments are shown in Table 2 and Fig. 14 (for solutions with a concentration of 5000 mg/L). Table 2 illustrates that the $K_{\rm W}'$ values of PDM and PDSM are significantly smaller than the $K_{\rm O}'$ values, indicating their ability to preferentially reduce the permeability of the water layer, i.e., water plugging without oil plugging. This is due to the adsorption of PDM and PDSM onto the negatively charged rock pore walls, where the hydrophilic groups act as adsorption anchors, dispersing in the water phase near the pore walls. This causes the polymer chains to hydrate and expand, reducing the effective pore size during water flow and thus increasing the resistance to water flow while reducing water layer permeability (Ahmed et al., 2023; Guo et al., 2014; Li et al., 2022b).

From Fig. 14, it is evident that PDSM significantly reduces water layer permeability compared to PDM and PSM. As a result, the standard water—oil flow resistance ratio ($N_{\rm FRR}$) for PDSM is 75.6% and 270.5% higher than that of PDM and PSM, respectively. This is because PDSM contains both cationic and hydrophobic groups. Hydrophobic groups promote intermolecular associations, enhancing the strength of the polymer's network structure and leading to more pronounced hydration and expansion of the polymer chain. At the same time, cationic groups allow polymer molecules to adsorb more tightly on the surface of rocks. The synergistic effect of these two interactions increases resistance to water flow, resulting in superior selective water control

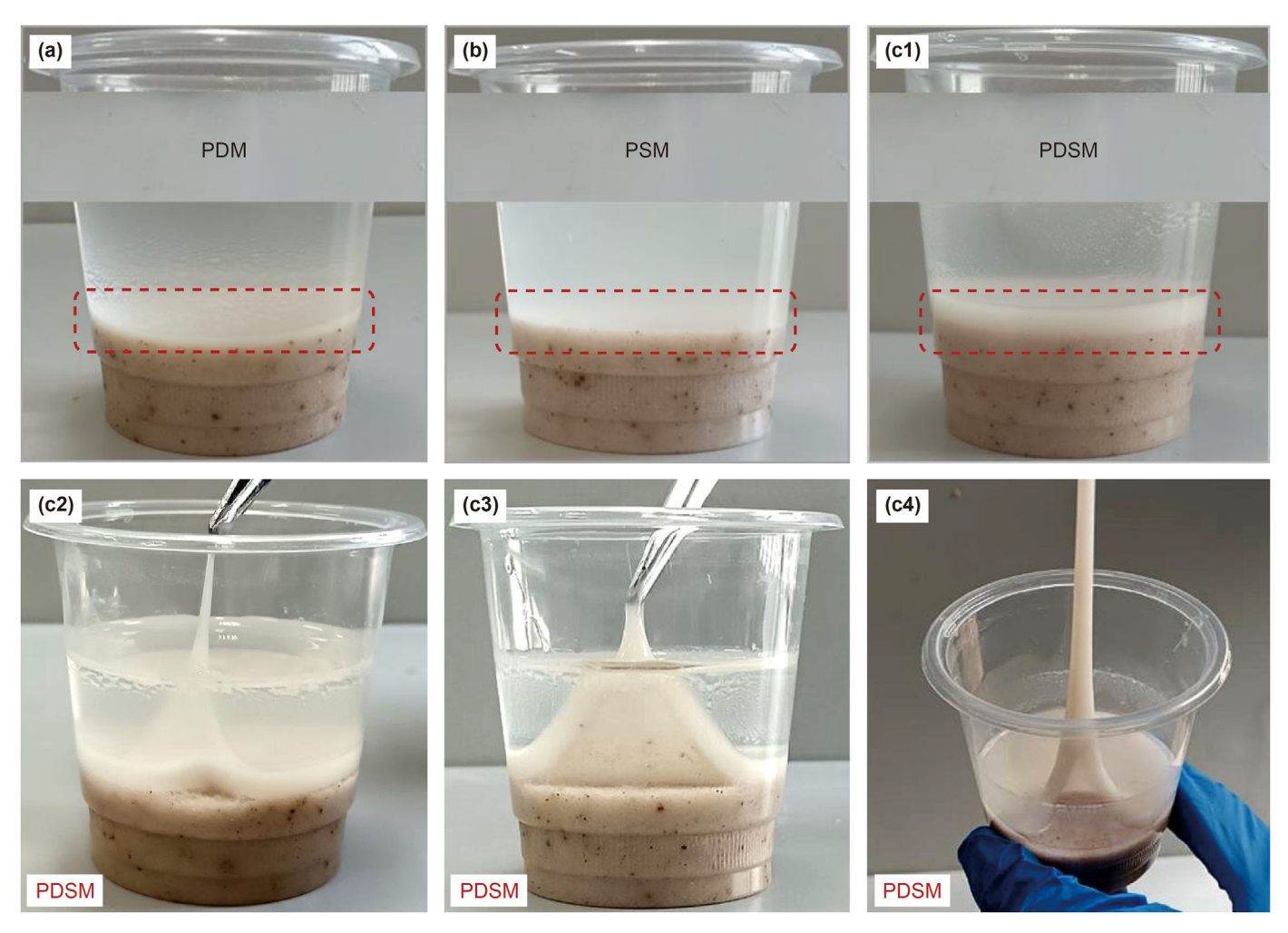


Fig. 13. Adsorption layer formed by PDM (a), PSM (b), and PDSM (c) on the surfaces of sand grains.

Table 2Core displacement experimental results of functional polymers.

Polymer	K _w	Ko	$K_{w}{}'$	K _o ′	F_{RRw}	$F_{\rm RRo}$	$N_{\rm FRR}$
PDM	2.52	1.34	0.72	1.18	3.500	1.136	3.08
PSM	2.46	1.42	1.38	1.16	1.783	1.224	1.46
PDSM	2.56	1.31	0.39	1.08	6.564	1.213	5.41

performance (Ahmed et al., 2023; Hayavi et al., 2023; Lai et al., 2013).

3.4.2. Reducing the water cut of produced fluid

In oilfield production, one of the most direct indicators of water control performance is the reduction in water cut (the ratio of water production to total liquid production from an oil well). A greater reduction in water cut indicates better water control performance. The ability of PSM, PDM, and PDSM to reduce the water cut in the produced fluid was studied, and the results are shown in Fig. 15.

When the functional polymer solution is injected in reverse, followed by forward water flooding, the injection pressure for both PDM and PDSM increases significantly, and the water cut decreases notably. This is due to that the functional polymers have selective water control performance, which allows them to preferentially enter the high permeability water flow channel and generate greater flow resistance to the water phase without affecting oil flow

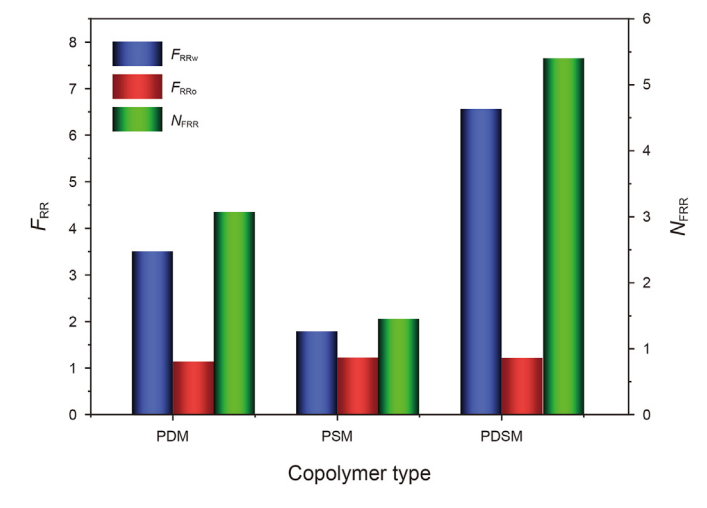


Fig. 14. F_{RR} and N_{FRR} values established by PSM, PDM, and PDSM.

(Askarinezhad et al., 2021; Hayavi et al., 2023; Lai et al., 2013). Compared to PDM and PSM, the injection pressure formed by PDSM generates higher injection pressures and results in a more pronounced reduction in the water cut of the produced fluid (PDSM: 96.1%–77.5%; PDM: 96.0%–83.7%; PSM: 96.1%–87.9%). PDSM

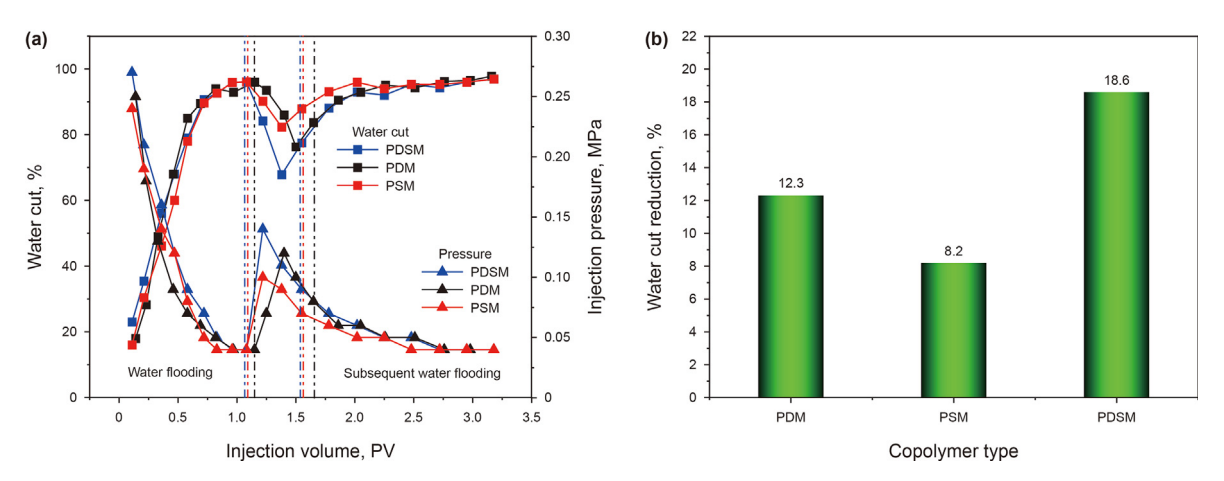


Fig. 15. Sand pipe displacement curves (a) and reductions in water cut (b) of produced fluids by PDM, PSM, PDSM.

establishes a higher resistance factor in porous media, resulting in better water layer permeability reduction, effectively preventing the advancement of the water phase, improving sweep efficiency, and achieving the dual effect of water control and oil stabilization (Abdullahi et al., 2022; Lei et al., 2022).

3.5. Mechanism analysis of sand-water dual-control

Loose sandstone reservoirs have formed a large number of highpermeability channels due to sand production and long-term water flooding, resulting in ineffective water injection cycles. Despite this, substantial residual oil remains trapped in the formation. When the functional polymer PDSM is injected, it preferentially enters these high permeability water flow channels. The mechanism of sand—water dual-control is shown in Fig. 16, where (a) represents polymer molecules adsorbing onto the surface of sand grains through electrostatic and hydrogen bonding interactions; (b) represents the formation of an intermolecular network structure through association; (c) illustrates polymer molecules adsorbing on the surface of the sand grains, agglomerating and bundling the sand particles through associative interactions; (d) depicts polymer molecules expanding in water and contracting in oil when adsorbed on the sand grain surface.

Quaternary ammonium and amide groups in PDSM are adsorbed on the surfaces of sand grains by electrostatic and hydrogen bonding interactions, respectively (Hayavi et al., 2023; Li et al., 2022c), forming an adsorption layer (polymer concentrated layer) (refer to Fig. 8(b), 9, and 13). The benzene ring strengthens the intermolecular network structure through the π - π interactions, thereby bridging and bundling the sand grains on the pore surface. Thus, the sand grains are agglomerated together to prevent them from detaching (refer to Figs. 10–12). In addition, PDSM molecules hydrate and expand in water, increasing the flow resistance of the water phase and reducing the water layer permeability. In contrast, PDSM molecules dehydrate and shrink when in contact with oil, which does not affect the flow of the oil phase and maintains the oil layer permeability (according to Table 2 and Fig. 14). This selective water control allows the subsequent water flooding to target the

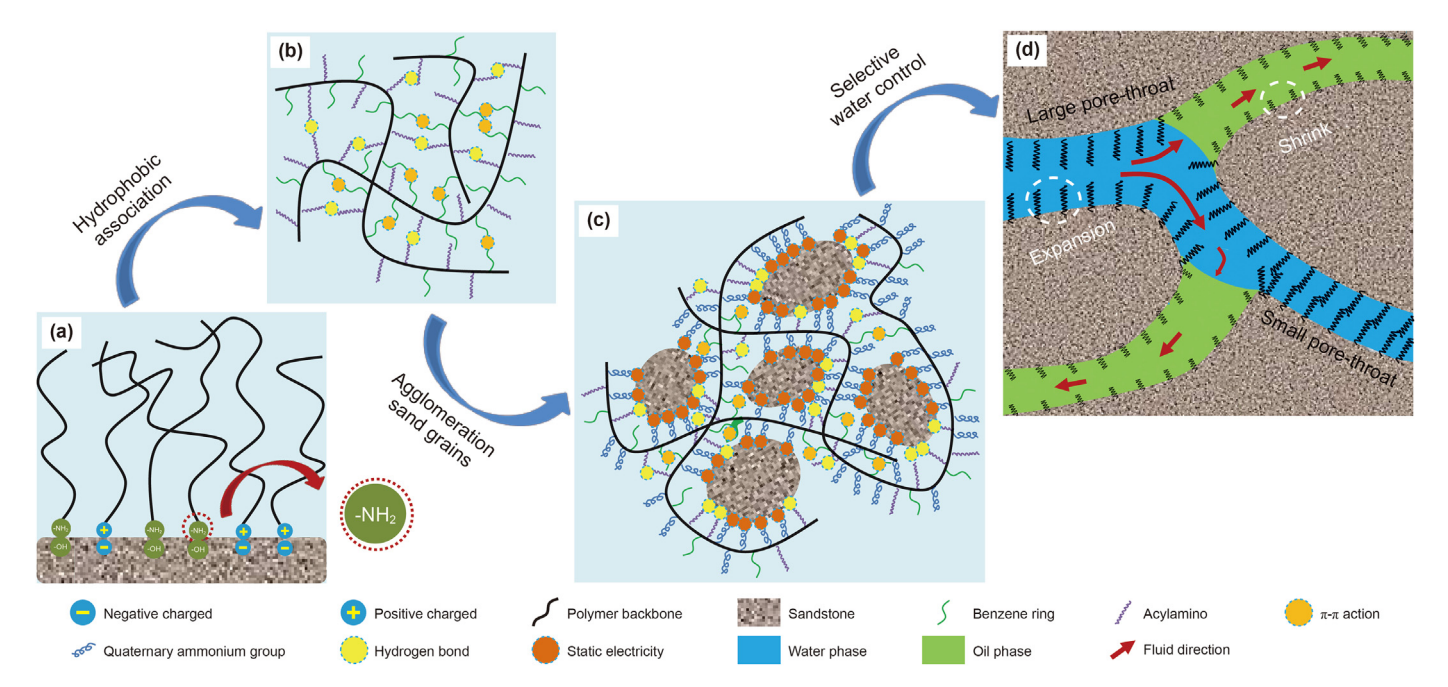


Fig. 16. Mechanism of sand—water dual-control by functional polymer PDSM.

low permeability zone previously unaffected, reducing the water cut in the produced liquid (as shown in Fig. 15).

In summary, the mechanism by which PDSM achieves effective sand—water dual-control is as follows. *Wettability alteration*: PDSM significantly reduces the contact angle of the water phase on the oil—wet rock surface to 64.0°, facilitating the adsorption and retention of functional polymer molecules on the pore surfaces. *Sand grain agglomeration*: PDSM bridges and bundles sand grains on pore surfaces through electrostatic, hydrogen bonding, and association interactions, enhancing the agglomeration of sand grains and improving their resistance to the erosive forces of fluid flow. *Selective water control*: PDSM forms an adsorption layer (polymer concentrated layer) on the pore surfaces, which expands in water and contracts in oil, thereby significantly reducing the water layer permeability without affecting the oil layer permeability.

4. Conclusions

To fully utilize the synergistic effects of functional monomers, DMC and SM were introduced into the polymer backbone to prepare a novel functional polymer PDSM with sand—water dual-control effects. The performance of PDSM was evaluated and compared against reference polymers, PDM and PSM, which contained only DMC or SM, respectively. The key conclusions are as follows.

- (1) The synergistic effect of DMC and SM significantly improved the wettability alteration and adsorption properties of PDSM on the rock surface, making it easier for its molecules to adsorb and retain. Compared to PDM and PSM, the static adsorption capacity of PDSM increased by 67.8% and 1725.0%, respectively, reaching 14.6 mg/g.
- (2) The incorporation of both functional monomers resulted in superior sand control performance for PDSM. Compared to PDM (284 s, 0.042 g/L, 12.5 mL/min) and PSM (51 s, 0.068 g/L, 8.0 mL/min), PDSM exhibited a 94.7% and 984.3% increase in sand leakage time (553 s), a 38.1% and 61.7% decrease in sand production (0.026 g/L), and a 28.0% and 100.0% increase in critical sand production flow rate (16.0 mL/min). According to the "Q/SH 1020 2377-2020" sand inhibitor evaluation standard, PDSM far exceeds the "excellent" performance requirement of a sand-production rate of ≤ 0.05 g/L.
- (3) Sand pipe displacement experiments demonstrated that PDSM offers a better selective water control effect. Compared to PDM (3.08) and PSM (1.46), the standard water—oil resistance ratio (*N*_{FRR}) of PDSM (5.41) increased by 75.6% and 270.5%, respectively. Additionally, the water cut of produced liquid was reduced by 6.3% and 10.4%, respectively. In summary, the synergistic effects of cations (DMC) and hydrophobic (SM) monomers significantly enhance sand—water dual-control performance, leading to more effective water control and oil stabilization.

CRediT authorship contribution statement

Tian-Meng Lei: Writing — original draft, Methodology, Investigation, Formal analysis, Conceptualization. **Ye-Fei Wang:** Writing — review & editing. **Xin-Fang Xue:** Software, Project administration. **Guo-Rui Xu:** Software, Formal analysis. **Ying-Ying Duan:** Software, Project administration. **Tian-Ci Ma:** Formal analysis. **Fu-Min Zhang:** Visualization, Validation. **Shi-Ze Qiu:** Software, Resources.

Declaration of competing interest

The authors declare that they have no conflict of interest.

Acknowledgements

This work was supported by the National Natural Science Foundation of China (General Program) (Grant No. 52474071). The authors appreciate the financial support from the China Scholarship Council (TM. Lei, No. 202406450004).

References

- Abdullahi, M.B., Jufar, S.R., Kumar, S., et al., 2022. Synergistic effect of polymeraugmented low salinity flooding for oil recovery efficiency in illite-sand. J. Mol. Liq. 358 (21), 119217–119230. https://doi.org/10.1016/ j.molliq.2022.119217.
- Ahmed, A.A., Saaid, I.M., Shafian, S.R.M., 2020. Novel relative permeability modifier using polymer grafted nanoclay. Energy Fuels 34 (3), 2703–2709. https:// doi.org/10.1021/acs.energyfuels.9b03500.
- Ahmed, A.A., Saaid, I.M., Sambo, C., et al., 2023. Experimental investigation and numerical simulation of relative permeability modifiers during water shut-off. Geoenergy Sci. Eng. 230 (12), 212095—212105. https://doi.org/10.1016/j.geoen.2023.212095.
- Ai-shajalee, F., Arif, M., Myers, M., et al., 2021. Rock/fluid/polymer interaction mechanisms: implications for water shut-off treatment. Energy Fuels 35 (16), 12809–12827. https://doi.org/10.1021/acs.energyfuels.1c01480.
- Alakbari, F.S., Mohyaldinn, F.S., Muhsan, A.S., et al., 2020. Chemical sand consolidation: from polymersto nanoparticles. Polymers 12 (42), 1069–1099. https://doi.org/10.3390/polym12051069.
- Askarinezhad, R., Hatzignatiou, D.G., Stavland, A., 2021. Associative polymers for disproportionate permeability reduction—formation wettability effects. J. Petrol. Sci. Eng. 206 (13), 109060–109074. https://doi.org/10.1016/ i.petrol.2021.109060.
- Chen, M.F., Wang, Y.F., Chen, W.H., et al., 2023. Synthesis and evaluation of multiaromatic ring copolymer as viscosity reducer for enhancing heavy oil recovery. Chem. Eng. J. 470 (25), 144220–144230. https://doi.org/10.1016/ i.cei.2023.144220.
- Chiappa, L., Mennella, A., Lockhart, T.P., et al., 1999. Polymer adsorption at the brine/rock interface: the role of electrostatic interactions and wettability. J. Petrol. Sci. Eng. 24 (2–4), 113–122. https://doi.org/10.1016/S0920-4105(99)00035-2.
- Dai, C.L., Zhao, G., You, Q., et al., 2014. The investigation of a new moderate water shutoff agent: cationic polymer and anionic polymer. J. Appl. Polym. Sci. 131 (3), 39462–39471. https://doi.org/10.1002/app.39462.
- Deng, F.C., Shen, X.F., Liang, Q.M., et al., 2018. The jamming mechanism of sand control screen for the montmorillonite inflation with the water. J. Pet. Explor. Prod. Technol. 8 (5), 189–194. https://doi.org/10.1007/s13202-017-0329-z.
- Fan, H.L., Wang, J.H., Tao, Z., et al., 2019. Adjacent cationic—aromatic sequences yield strong electrostatic adhesion of hydrogels in seawater. Nat. Commun. 10 (1), 5127–5135. https://doi.org/10.1038/s41467-019-13171-9.
- Gebbie, M.A., Wei, W., Schrader, A.M., et al., 2017. Israelachvili, Tuning underwater adhesion with cation—π interactions. Nat. Chem. 9 (5), 473–479. https://doi.org/10.1038/nchem.2720.
- Guo, A.J., Geng, Y.R., Zhao, L.L., et al., 2014. Preparation of cationic polyacrylamide microsphere emulsion and its performance for permeability reduction. Petrol. Sci. 11 (5), 408–416. https://doi.org/10.1007/s12182-014-0355-0.
- Hayavi, M.T., Kalantariasl, A., Malayer, M.R., 2023. Application of polymeric relative permeability modifiers for water control purposes: opportunities and challenges. Geoenergy Sci. Eng. 231 (8), 212330–212369. https://doi.org/10.1016/ j.geoen.2023.212330.
- Howard, G.J., Hudson, F.L., West, J., 1977. Water-soluble polymers as retention aids in a model papermaking system. I. polyacrylamides. J. Appl. Polym. Sci. 21 (1), 1–16. https://doi.org/10.1002/app.1977.070210101.
- Huang, X.B., Shen, H.K., Sun, J.S., et al., 2018. Nanoscale laponite as a potential shale inhibitor in water-based drilling fluid for stabilization of wellbore stability and mechanism study. ACS Appl. Mater. Interfaces 10 (39), 33252–33259. https:// doi.org/10.1021/acsami.8b11419.
- Ivšinović, J., Pleteš, V., Babić, V., 2022. Sand management of small hydrocarbon mature fields: single well case study on field in the western part of the Sava Depression (Croatia). Petrol. Sci. Technol. 40 (9), 1019–1032. https://doi.org/ 10.1080/10916466.2021.2009511.
- Lai, N.J., Qin, X.P., Ye, Z.B., et al., 2013. The study on permeability reduction performance of a hyperbranched polymer in high permeability porous medium. J. Petrol. Sci. Eng. 112 (24), 198–205. https://doi.org/10.1016/j.petrol.2013.11.005.
- Lei, T.M., Cao, J., Li, A.F., et al., 2024. Synthesis and oil displacement performance evaluation of a novel functional polymer for heavy oil recovery. J. Mol. Liq. 402 (32), 124746–124754.
- Lei, T.M., Wang, Y.F., Zhang, H., et al., 2022. Preparation and performance evaluation

- of a branched functional polymer for heavy oil recovery. J. Mol. Liq. 363 (17), 119808—119818. https://doi.org/10.1016/j.molliq.2022.119808.
- Li, J.D., Zhang, G.C., Ge, J.J., et al., 2022a. Self-aggregating behavior of poly(4-vinyl pyridine) and the potential in mitigating sand production based on $\pi-\pi$ stacking interaction. Petrol. Sci. 19 (5), 2165–2174. https://doi.org/10.1016/j.petsci.2022.06.001.
- Li, J.D., Zhang, G.C., Ge, J.J., et al., 2022b. Self-healing elastomer modified proppants for proppant flowback control in hydraulic fracturing. Petrol. Sci. 19 (1), 245–253. https://doi.org/10.1016/j.petsci.2021.12.025.
- Li, L., Smitthipong, W., Zong, H.B., 2015. Mussel-inspired hydrogels for biomedical and environmental applications. Polym. Chem. 6 (3), 353–358. https://doi.org/ 10.1039/C4PY01415D.
- Li, X.Q., Zhang, G.C., Ge, J.J., et al., 2017. Organosilane film for sand migration control based on in-situ hydrolysis and polycondensation effects. J. Petrol. Sci. Eng. 158 (17), 660–671. https://doi.org/10.1016/j.petrol.2017.08.013.
- Li, Z., Kang, W.L., Yang, H.B., et al., 2022c. Advances of supramolecular interaction systems for improved oil recovery (IOR). Adv. Colloid Interface Sci. 301 (24), 102617–102640. https://doi.org/10.1016/j.cis.2022.102617.
- Liu, D.X., Zhong, X., Shi, X.F., et al., 2016. Pentaerythritol phosphate melamine salt, a new aggregating reagent for oilfield chemical sand control: preparation, properties, and mechanism. Energy Fuels 30 (3), 2503–2513. https://doi.org/10.1021/acs.energyfuels.5b02648.
- Luo, Q., Tang, K., Bai, L., et al., 2022. Development of in-situ starch grafted copoly-merized gels for conglomerate reservoir conformance control and oil recovery improvement. J. Petrol. Sci. Eng. 210 (9), 110005–1100016. https://doi.org/10.1016/j.petrol.2021.110005.
- Marandi, S.Z., Salehi, M.B., Moghadam, A.M., et al., 2018. Sand control: experimental performance of polyacrylamide hydrogels. J. Petrol. Sci. Eng. 170 (32), 430–439. https://doi.org/10.1016/j.petrol.2018.06.074.
- Mishra, S., Ojha, K., 2016a. Application of an improvised inorganic—organic chemical mixture to consolidate loose sand formations in oil fields. J. Petrol. Sci. Eng. 137 (6), 1–9. https://doi.org/10.1016/j.petrol.2015.11.008.
- Mishra, S., Ojha, K., 2016b. Nanoparticle induced chemical system for consolidating loosely bound sand formations in oil fields. J. Petrol. Sci. Eng. 147 (19), 15–23. https://doi.org/10.1016/j.petrol.2016.05.005.
- Nejati, H., Khamehchi, E., Derakhshan, A.A., et al., 2023. Synthesis and optimization of a novel epoxy-based nanofluid for sand consolidation in oil wells. Geoenergy Sci. Eng. 230 (12), 212217–212231. https://doi.org/10.1016/j.geoen.2023.212217.
- Pereira, A.Z.I., Delpech, M.C., 2012. Thermal and mechanical evaluation of the stability of recycled poly(ethylene terephthalate) applied as sand control agent in petroleum wells. Polym. Degrad. 97 (7), 1158–1163. https://doi.org/10.1016/j.polymdegradstab.2012.03.045.
- Qiao, R., Zhu, W.Q., 2010. Evaluation of modified cationic starch for impeding polymer channeling and in-depth profile control after polymer flooding. J. Ind. Eng. Chem. 16 (2), 278–282. https://doi.org/10.1016/j.jiec.2009.09.070.
- Qin, L.M., Arjomand, E., Myers, M.B., et al., 2020. Mechanistic aspects of polymeric relative permeability modifier adsorption onto carbonate rocks. Energy Fuels 34 (10), 12065—12077. https://doi.org/10.1021/acs.energyfuels.0c01590.
- Ross, C.M., Rangel-German, E.R., Castanier, L.M., et al., 2006. A laboratory investigation of temperature-induced sand consolidation. SPE J. 11 (52), 206–215. https://doi.org/10.2118/92398-MS.

- Safaei, A., Asefi, M., Ahmadi, M., et al., 2023. Chemical treatment for sand production control: a review ofmaterials, methods, and field operations. Petrol. Sci. 20 (3), 1640–1658. https://doi.org/10.1016/j.petsci.2023.02.013.
- Saghandali, F., Salehi, M.B., Hosseinzadehsemnani, R., et al., 2022. A review on chemical sand production control techniques in oil reservoirs. Energy Fuels 36 (10), 5185–5208. https://doi.org/10.1021/acs.energyfuels.2c00700.
- Seright, R., Brattekas, B., 2021. Water shutoff and conformance improvement: an introduction. Petrol. Sci. 18 (35), 450–478. https://doi.org/10.1007/s12182-021-00546-1
- Shi, L.T., Zhu, S.J., Ye, Z.B., et al., 2020. The seepage flow characteristics of hydrophobically associated polymers with different aggregation behaviours in porous media. R. Soc. Open Sci. 7 (1), 191270–191285. https://doi.org/10.1098/1505.191270.
- Sun, X.D., Bai, B.J., Long, Y.F., et al., 2020a. A comprehensive review of hydrogel performance under CO2 conditions for conformance control. J. Petrol. Sci. Eng. 185 (28), 106662–106674. https://doi.org/10.1016/j.petrol.2019.106662.
- Sun, X.D., Long, Y.F., Bai, B.J., et al., 2020b. Evaluation and plugging performance of carbon dioxide-resistant particle gels for conformance control. SPE J. 25 (4), 1745–1760, https://doi.org/10.2118/200493-PA.
- Tabar, M.A., Bagherzadeh, H., Shahrabadi, A., et al., 2021. A comprehensive research in chemical consolidator/stabilizer agents on sand production control. J. Pet. Explor. Prod. Technol. 11 (12), 4305–4324. https://doi.org/10.1007/s13202-021-01303-1.
- Wang, J., Zhu, X.Y., Guo, H.Y., et al., 2011. Synthesis and behavior evaluation of a relative permeability modifier. J. Petrol. Sci. Eng. 80 (1), 69–74. https://doi.org/10.1016/j.petrol.2011.10.013.
- Ye, Z.B., He, E.Q., Xie, S.Y., et al., 2010. The mechanism study of disproportionate permeability reduction by hydrophobically associating water-soluble polymer gel. J. Petrol. Sci. Eng. 72 (1–2), 64–66. https://doi.org/10.1016/j.petrol.2010.03.004.
- Zhao, G., Dai, C.L., Chen, A., et al., 2015. Experimental study and application of gels formed by nonionic polyacrylamide and phenolic resin for in-depth profile control. J. Petrol. Sci. Eng. 135 (32), 552–560. https://doi.org/10.1016/ j.petrol.2015.10.020.
- Zhao, J., Fan, H.F., You, Q., et al., 2017. Distribution and presence of polymers in porous media. Energies 10 (12), 2118–2131. https://doi.org/10.3390/en10122118.
- Zhu, D., Peng, S., Zhao, S., et al., 2021a. Comprehensive review of sealant materials for leakage remediation technology in geological CO₂ capture and storage process. Energy Fuels 35 (6), 4711–4742. https://doi.org/10.1021/acs.energyfuels.0c04416.
- Zhu, D., Xu, Z., Sun, R., et al., 2021b. Laboratory evaluation on temporary plugging performance of degradable preformed particle gels (DPPGs). Fuel 289 (52), 119743–119754. https://doi.org/10.1016/j.fuel.2020.119743.
- Zhu, D.Y., Deng, Z.H., Chen, S.W., 2021c. A review of nuclear magnetic resonance (NMR) technology applied in the characterization of polymer gels for petroleum reservoir conformance control. Petrol. Sci. 18 (6), 1760–1775. https://doi.org/ 10.1016/j.petsci.2021.09.008.
- Zhu, S.J., Ye, Z.B., Liu, Z.H., et al., 2021d. Adsorption characteristics of polymer solutions on media surfaces and their main influencing factors. Polymers 13 (11), 1774–1788. https://doi.org/10.3390/polym13111774.